Environmental Science and Pollution Research
https://doi.org/10.1007/s11356-023-26627-9

PERCEPTIONS IN GROUNDWATER CONTAMINATION, RISK ASSESSMENT, AND MANAGEMENT STRATEGIES

Development of Bi_2S_3/Cu_2S hetrojuction as an effective photocatalysts for the efficient degradation of antibiotic drug and organic dye

Balaji Parasuraman[1] · Vasanthakumar Vasudevan[2] · Bhuvaneswari Kandasamy[3] · Hariprasath Rangaraju[1] · Pazhanivel Thangavelu[1]

Received: 31 January 2023 / Accepted: 20 March 2023

Abstract

Herein, a Bi_2S_3/Cu_2S was successfully synthesized via a simple one-step wet impregnation process. The compositional behavior and electrical and optical properties of photocatalysts were investigated in detail. Photocatalytic technology has shown great promise in wastewater treatment, splitting water to hydrogen, and converting CO_2 to fuel. Researchers or scientist are attempting to design sulfate-based heterojunction photocatalytic systems in order to develop novel photocatalysts with excellent performance. Photodegradation of methylene blue (MB) dye and tetracycline (TC) drug under visible light irradiation was used to assess the photocatalytic activity of as-prepared samples. As a result, 2:1% wt of Bi_2S_3/Cu_2S heterostructure composite revealed superior visible light degradation performing of MB dye, and TC drug efficiency as 90.2% and 87.5%, respectively. The prepared hybrid photocatalyst has demonstated a potential for use in the photocatalytic degradation of antibiotic durgs and dyes, indicating a promissing future for its application.

Keywords Photodegradation activity · Hydrothermal process · Dye and drug degradation · Recycling stability · Scavengers

Introduction

Environmental pollution has become an apparent threat to the current generation, at present access to non-contaminated water and other environmental resources have become a comprehensive challenge for humanity (Cui et al. 2017). Water resources have been heavily polluted in recent decades by incorporating massive amounts of various synthetic dyes (Mrunal et al. 2019), pharmaceuticals drugs (Majumder et al. 2020), pesticides (Moradeeya et al. 2022), personal care products, and other industrial chemicals (Oluwole et al. 2020) (Tayyab et al. 2022a). The increased population, global industrialization, and over-exploitation of hazardous chemicals have become major reasons for reduced potable water sources (Bhuvaneswari et al. 2021a). The discharge of these toxic compounds in the water reservoirs is not only harmful to human health but also causes damage to marine ecosystems (He et al. 2021). For example, some drugs have been widely used to COVID-19 pandemic, according to WHO reports, there have been 250 million cases of COVID-19 confirmed by PCR-based tests, including 5 million deaths to date, despite widespread use of potentially harmful mediators. Sneezing, coughing, face to face chatting, and any other unhealthy activity can result in virus transmission. This widespread use

Responsible Editor: George Z. Kyzas

Highlights
- Bi_2S_3/Cu_2S nanocomposites were synthesized by a simple one-step wet impregnation method.
- The photodegradation of methylene blue (MB) dye and tetracycline drug (TC) has been analyzed.
- The prepared Bi_2S_3/Cu_2S nanocomposites showed enhanced photocatalytic activity, removing 90.2% of MB dye and 87.5% TC drug, respectively.

✉ Pazhanivel Thangavelu
pazhanit@gmail.com

[1] Smart Materials Laboratory, Department of Physics, Periyar University, Salem 636011, Tamil Nadu, India

[2] Xiamen Key Laboratory of Municipal and Industrial Solid Waste Utilization and Pollution Control, College of Civil Engineering, Huaqiao University, Xiamen, Fujian 361021, People's Republic of China

[3] Department of Materials Engineering, Kasetsart University, Bangkok 10903, Thailand

Published online: 05 April 2023

of coronavirus-fighting drugs will undoubtedly pollute our environment and harm the ecosystem (Ebrahimi and Akhavan 2022). In order to pressing need for clean and safe drinking water, it is essential to treat pollutants to maintain water quality (Tayyab et al. 2022c). The photocatalysis technology has been quickly developed in treating wastewater in recent years because of its outstanding performance characteristics such as environmental friendliness (Yu et al. 2022), high energy efficiency (Liu et al. 2021b), and lack of secondary pollution (Chong et al. 2010). It has emerged as an important method, because of its fast and complete mineralization of contaminants without leaving residues (Tayyab et al. 2022b).

Semiconductor materials (Jia et al. 2019) have been broadly used in numerous applications such as supercapacitors (Ali et al. 2018), gas sensors (Marimuthu et al. 2021), hydrogen evaluation (Ye et al. 2022), biosensors (Chaniotakis and Sofikiti 2008), photocatalysts (Cui et al. 2017), antibacterial (Nourmohammadi et al. 2014), and antiviral (Akhavan et al. 2010). Many semiconductor metal oxides such as TiO_2 (Mahmoodi et al. 2006), ZnO (Hariharan 2006), Bi_2O_3 (Sonkusare et al. 2018), In_2O_3 (Shchukin et al. 2004), SnO_2 (Elango and Roopan 2016), Fe_2O_3 (Li et al. 2015), Ag_3PO_4 (Liu et al. 2013), $FeWO_4$ (Dadigala et al. 2019), and $lnMoO_3$-TiO_2 (Jada et al. 2021) and sulfides such as ZnS (Ravikumar et al. 2022), CdS (Das and Ahn 2022), MoO3, and MoS_2 (Saadati et al. 2021) are mostly used semiconductors. In particular, heterogeneous photocatalyst has enormous research interest in the last few decades, and TiO_2 was the focus of many early research activities. These materials have attracted attention due to their definite bandgap between the valence and conduction bands. However, their huge application is limited due to the fast recombination of photo-generated electron–hole pairs (Bhuvaneswari et al. 2021b). It is observed that when the rate of electron–hole pair recombination is minimum, the photocatalytic efficiency of photocatalysts is high. Different alternatives are used to increase the photocatalytic activity of these materials (Liu et al. 2021a), including doping ions into the photocatalysts and coupling them with other semiconductors, forming a heterostructure (Wei et al. 2018). Optimization of heterostructures through bandgap regulation helps to improve both visible light utilization and photogenerated charge carrier separation, resulting in a photocatalyst with a high efficiency. Lamellar-shaped compound, hydrophilic property (Zhao et al. 2017), bismuth sulfide (Bi_2S_3) is a typical p-type semiconductor that has a band gap of approximately 1.3 eV (Ajiboye and Onwudiwe 2021). Ravindranadh Koutavarapu et al. synthesized $NaBiS_2$/ZnO nanomaterials through the hydrothermal method and prepared various compositions which enabled maximum photodegradation of TC drug under the influence of UV–visible light irradiation with high stability and reusability. On the other hand, the combination of $NaBiS_2$/ZnO hetero-structure has notably improved the movement of charge carriers at the boundary to obstruct the recombination of photoexcited charge carriers thus improving the photodegradation of TC. In recent years, various synthesis methods have been used to create Bi_2S_3 nanostructures with various morphologies, such as nanotubes, nanorods, nanowires, nanoflowers, and nanocomposites. For example, Deqiang Zhao et al. investigated a visible light driven Bi_2S_3/$BiVO_4$ nanocomposite synthesized by a hydrothermal method; Shouning Yang et al. examined two-dimensional BiOCl-Bi_2S_3-Cu_2S ternary nanocomposites prepared by one-pot hydrothermal method which were using bacterial disinfection. The heterostructure was studied as a catalyst for rhodamine B (RhB) degradation and possible formation and degradation mechanisms that are strongly affected by pH under visible light irradiation were proposed. The findings suggest that this hetro structured material could be used in environmental and energy applications (Danish et al. 2020). (Palanisamy et al. 2020). To date, some breakthrough has been made in the field of Cu_2S acting as a catalysts; Qian Wang et al. created a GO/Cu_2S nanostructure with enhanced photocatalytic activity when exposed to visible light. Most researchers focus on cellulose fibers with hyper branched polyamide-amine and linear CuS nanomaterials (Xu et al. 2015). Therefore, consequently, it is possible to incorporate suitable n-type semiconductor materials to promote the catalytic activity of p-type catalysts, n-type Bi_2S_3, and p-type Cu_2S which have been demonstrated to be effective photocatalysts (Elmetwally et al. 2021). In this article, the preparation of Bi_2S_3/Cu_2S nanostructures through a simple impregnation method was discussed in detail. XRD, FTIR, UV-DRS, SEM, EDS, HETEM, and XPS were used to investigate the optical, chemical, and structural properties of the nanocomposites. As-prepared samples were subjected to photo-degeneration of MB dyes and TC drugs; the possible reaction mechanism for photocatalytic activity enrichment was investigated.

Materials and methods

Chemicals and reagents

Sodium thiosulphate pentahydrate ($Na_2S_2O_3.5H_2O$), bismuth (III) nitrate pentahydrate (Bi $(NO_3)_3.5H_2O$), cupric nitrate trihydrate (Cu $(NO_3)_2.3H_2O$), thiourea (CH_2N_4S), silver nitrate ($AgNO_3$) ammonium oxalate $(NH_4)_2.C_2O_4$ and acetone (CH_3COCH_3), ethanol (C_2H_5OH), triethyl ammonium acetate $(CH_3CH_2)_3.NHOCOCH_3$ and MB. All the chemical purchased from Sigma-Aldrich. All compounds were used as obtained without purification.

Preparation of Bi_2S_3

In typical experiments, 12 g of $Na_2S_2O_3.5H_2O$ was dissolved in 60 ml of double distilled water (DDW) followed

by continued stirring, 3 g of $Bi(NO_3)_3.5H_2O$ is added to the precursor solution and after 30 min of stirring, the mixed solution was transferred to a 100 ml Teflon-lined stainless autoclave, the pH is kept around 12, and the temperature is kept at 60 °C for 12 h in a heated air oven and normally warmed to room temperature. Finally, the dark samples were taken and washed with multiple times DDW and ethanol.

Preparation of Cu_2S

In a typical synthesis, 3.8 g of Cu $(NO_3)_2.3H_2O$ and 1.58 g CH_2N_4S were mixed and stirred for 30 min in 40 ml of DDW. After that, the solution was sealed in a 100 ml Teflon-lined steel reaction vessel and heated in an oven at 180 °C for 12 h. After the reaction, the autoclave was made to attain room temperature and the precipitates were washed several times with DDW and ethanol. Finally, the products were centrifuged and dried at 80 °C.

Preparation of Bi_2S_3/Cu_2S nanocomposite

The wet impregnation method was used to build the Bi_2S_3/Cu_2S nanocomposite. Separately 1:1 and 2:1 weight ratios of Bi_2S_3 and Cu_2S are added to 10 ml of Ethanol. The obtained products were continuously stirred after the solution was heated up to 60 °C to evaporate the solvent in a hot air oven. Finally, the dried powder was used to further analysis.

Materials characterization

The structure and formation of the (2:1) Bi_2S_3/Cu_2S nanocomposite were confirmed using XRD analysis (XRD-Rigaku Smart Lab diffractometer). All of the functional groups of the as-prepared samples were confirmed by the FTIR (Perkin-Elmer Fourier transform spectrometer). The SEM and elemental composition analysis were obtained by Carl Zeiss Sigma, Germany. Elemental composition was obtained and the chemical composition of the (2:1) Bi_2S_3/Cu_2S nanocomposite was EDAX (FEI Quanta FEG 200), high-resolution transmission electron microscope (HRTEM, JOEL JEM 2001) was used to investigate the morphology, and XPS (PHI 5000 Versa Probe III) analysis was confirmed by the nanocomposite formation. The optical properties of the synthesized samples were confirmed using UV-visible spectroscopy (Perkin Elmer LAMBDA 950 UV-visible model spectrophotometer).

Photocatalytic evaluation

The photocatalytic investigation was conducted under UV-visible light irradiation, by using a halogen lamp (λ=420 nm, 86 W) as the light source. In a typical photocatalytic degradation procedure, 50 ml of MB (10 mg/L) dye solution was treated with (2:1) Bi_2S_3/CuS_2 in a 100 ml beaker and the suspension was maintained in darkness condition for 30 min to achieve the desorption/adsorption balance. The reaction suspension was then illuminated with UV light while the distance between the sample and the Xe lamp was held constant at 15 cm. The 3 ml of solution was withdrawn and centrifuged to split the photocatalyst. To detect photodegradation, the concentration of MB solution was measured using a UV-vis spectrophotometer at 664 nm. The degradation percentage was calculated using beer lambert relation (Rajendran et al. 2018).

$$\text{Degradation } (\%) = \left(C_0/C\right)/C_0 * 100 \quad (1)$$

where C_0 is the initial concentration of MB dye solution, C is the final concentration of MB dye solution, and T is the time (t).

Result and discussion

Powder X-ray diffraction analysis (PXRD)

To understand the crystallinity, crystal phase and composition of the as-prepared samples were performed by the PXRD and the obtained patterns are depicted in Fig. 1. The orthorhombic structure of Bi_2S_3 was observed by the lattice plane (0 2 0), (2, 1 0), (2 2 0), (1 1 1), (2 2 1), (2 4 0), (1 4 1), and (5 4 2) with its corresponding 2 theta values of 15.59°, 17.54°, 23.74°, 25.03°, 31.76°, 35.63°, 40.03°, and 71.09°, respectively. All of the diffraction peaks agree well with matched pure orthorhombic Bi^2S^3 (JCPDS #65-2435), and no additional peaks are observed, which indicates the absence of impurities (Ma et al. 2014). In Fig. 1, the observed diffraction peaks can be attributed to a pure Cu_2S

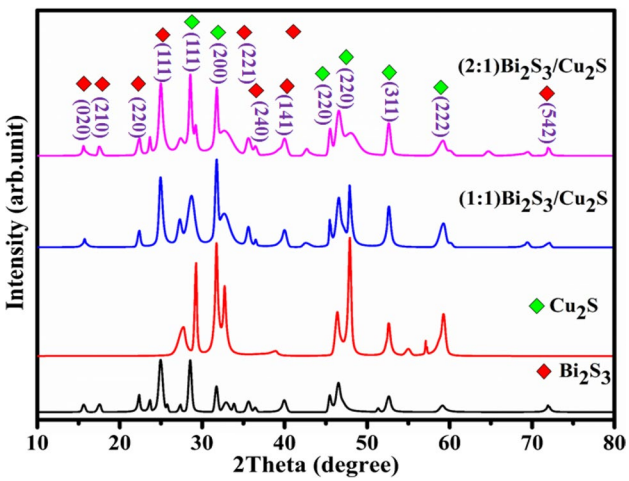

Fig. 1 XRD pattern of as-prepared samples

cubic structure with (1 1 1), (2 0 0), (220), (3 1 1), and (2 2 2) planes corresponding to 2 theta value of 29.01°, 31, 76°, 46.05°, 52.44°, and 57.10° in good agreement with (JCPDS #84-1770) (Mondal et al. 2015). X-ray diffraction patterns of Bi_2S_3/Cu_2S nanocomposites show the presence of both Bi_2S_3 and Cu_2S, which confirms the presence of the composite. Moreover, when Bi_2S_3 was added to Cu_2S nanoparticles, a decrease in the intensity of the diffraction peak (2 2 0) is noticed. To determine the crystal size of nanocomposites, the Debye–Scherer equation is used (Zhu et al. 2001). The calculated crystalline sizes of the Bi_2S_3, Cu_2S, Bi_2S_3/CuS_2 (1:1), and Bi_2S_3/CuS_2 (2:1) nanocomposites are 32.08, 18.47, 24.9, and 11.29 nm, respectively.

Fourier transform infrared spectroscopy (FTIR)

To investigate the functional groups, all the as-prepared samples were examined through FTIR spectroscopy and the result are depicted in Fig. S2. The stretching vibration of H_2O is responsible for a wide band around 3791 cm^{-1}, and the stretching mode of the absorbed CO_2 is represented by the peak centered around 1617 cm^{-1}. The band observed at 1385 cm^{-1} ascribed to the carboxyl O-H stretching. The peak at 1098 cm^{-1} represents the bending vibration of the C-O bond, and the weak peak around 2920 cm^{-1} represents the C-H bond of -CH3 groups; the peaks at 600 cm^{-1} and 1049 cm^{-1} may be due to C-S and C-N stretching vibrations, respectively (Arumugam et al. 2017).

Morphology analysis

SEM analysis

To investigate the morphology of the as-prepared nanocomposites, SEM analysis was performed and the observed results are displayed in Fig. 2a–d. The observed image of the as-prepared (2:1) Bi_2S_3/Cu_2S sample shows the deposition of irregularly with heavy agglomeration. This result exhibited the strong interaction between the Cu_2S and Bi_2S_3. Furthermore, in urchin-like microspheres (Zhou et al. 2014), the interaction of Bi_2S_3 and Cu_2S results in the formation of hybrid nanoparticles (Bharathi et al. 2019). These interactions help improve the charge separation and transfer characteristics of the nanocomposites; as a result, the photocatalytic activity for MB dye and TC drug degradation efficiency are improved.

HRTEM analysis

The corresponding HRTEM image of the as-prepared nanocomposites (2:1) Bi_2S_3/Cu_2S heterojunction is revealed in Fig. 3, the lattice distance of Bi_2S_3 is 0.2741 nm, which matched well with the (111) plane of Bi_2S_3, the $d = 0.2319$ nm distinct fringes correspond to the (200) crystallographic planes of Cu_2S. It can be clearly seen that there is an interference region, HRTEM analysis could determine that the heterojunction can be formed, and the lattice fringes also clearly indicate that the catalysts have good crystallinity of the as-prepared sample (Kuo et al. 2018).

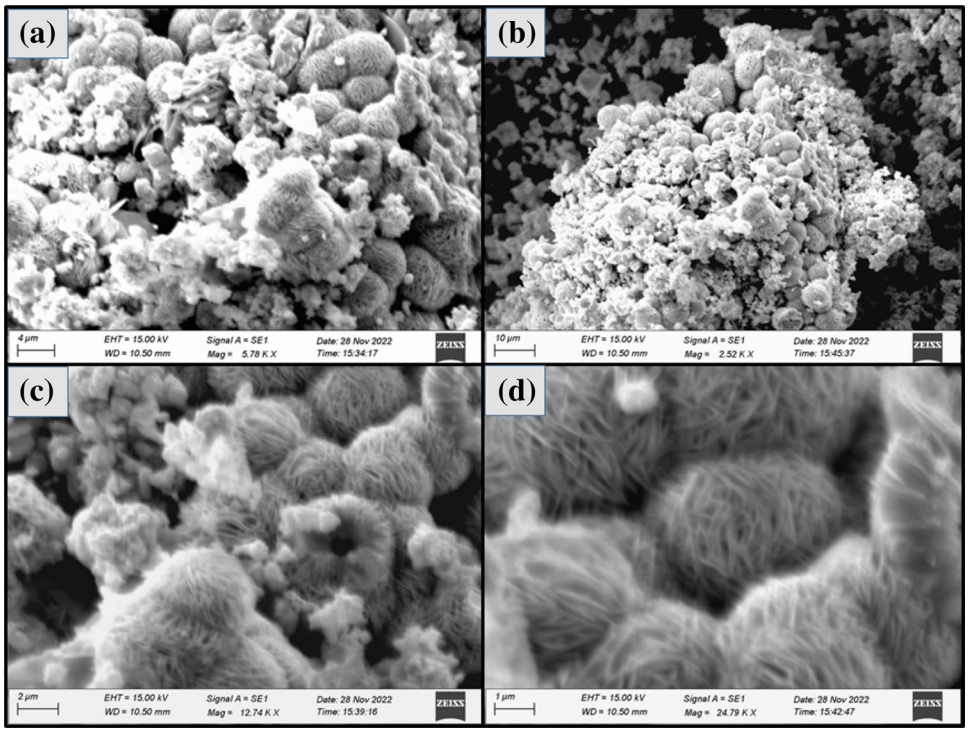

Fig. 2 **a–d** SEM image of the (2:1) Bi_2S_3/Cu_2S nanocomposites with different magnifications

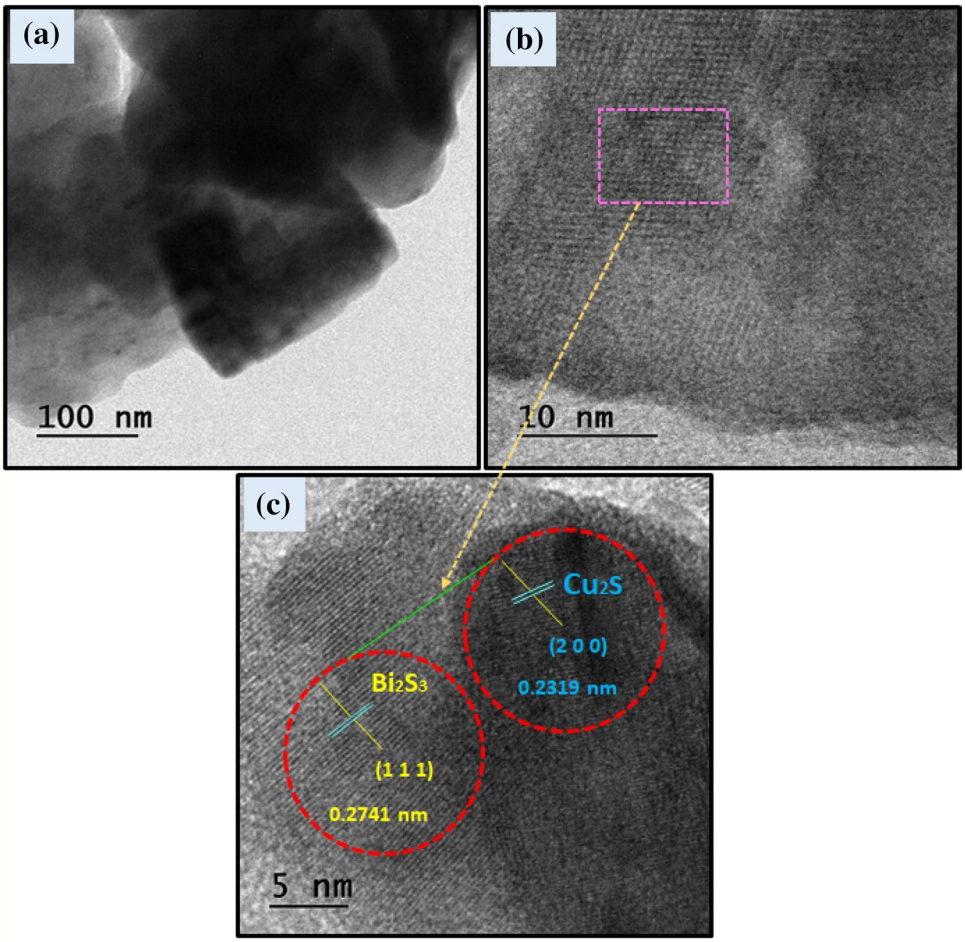

Fig. 3 **a**–**d** HRTEM image of the (2:1) Bi_2S_3/Cu_2S nanocomposites

UV- DRS analysis

The UV-visible absorption characteristics of Bi_2S_3, Cu_2S, (1:1) Bi_2S_3/Cu_2S, and (2:1) Bi_2S_3/Cu_2S were examined by using UV-visible absorption spectroscopy in Fig. S3 which displays the UV-visible absorption spectra of the as-prepared nanocomposites. The (2:1) Bi_2S_3/Cu_2S nanocomposites demonstrate greater absorption in the visible region, which could also improve photocatalytic activity under the influence of visible light irradiation. The energy bandgap (Eg) is one of the optical properties that explain the semiconductor nature of nanocomposites. Therefore, the band gap values were obtained from the plot of Tauc (αhυ) versus hυ, as shown in Fig. 4, and were calculated from the Eq. (2), the Tauc relation (Kumar et al. 2020):

$$(\alpha h\nu) = \alpha h\nu = A\,(h\nu - Eg)^{n} \quad (2)$$

In which h, v, and α denote the planks constant, light frequency, and absorption coefficient, respectively. The calculated energy band gap values of Bi_2S_3, Cu_2S, (1:1) Bi_2S_3/Cu_2S, and (2:1) Bi_2S_3/Cu_2S nanocomposites are 2.03, 1.83, 1.77, and 1.51 eV, respectively. The difference in band gap between pure Bi_2S_3, Cu_2S, and (1:1) Bi_2S_3/Cu_2S during the formation of nanocomposites (2:1) Bi_2S_3/Cu_2S confirms the hybrid formation.

Elemental mapping and energy dispersive X-ray analysis

The elemental mapping of (2:1) Bi_2S_3/Cu_2S nanocomposites has even distribution of Bi, Cu, O, and S elements in the Fig. S4. The sample purity was investigated by the elemental analysis of (2:1) Bi_2S_3/Cu_2S nanocomposites by using EDX spectroscopy revealed in the Fig. S5, which indicates the presence of Bi, Cu, O, and S in the (2:1) Bi_2S_3/Cu_2S nanocomposites in desired ratios.

X-ray photoelectron spectroscopy

The surface chemical composition of the as-prepared nanocomposites was examined by using XPS analysis. The XPS survey spectra of Bi_2S_3/Cu_2S nanocomposites indicate the presence of Bi, Cu, and S elements and their consequent binding energy peaks appear at corresponding positions as represented in Fig. 5. Bi $4f_{7/2}$ and Bi $4f_{5/2}$ emerge at 160

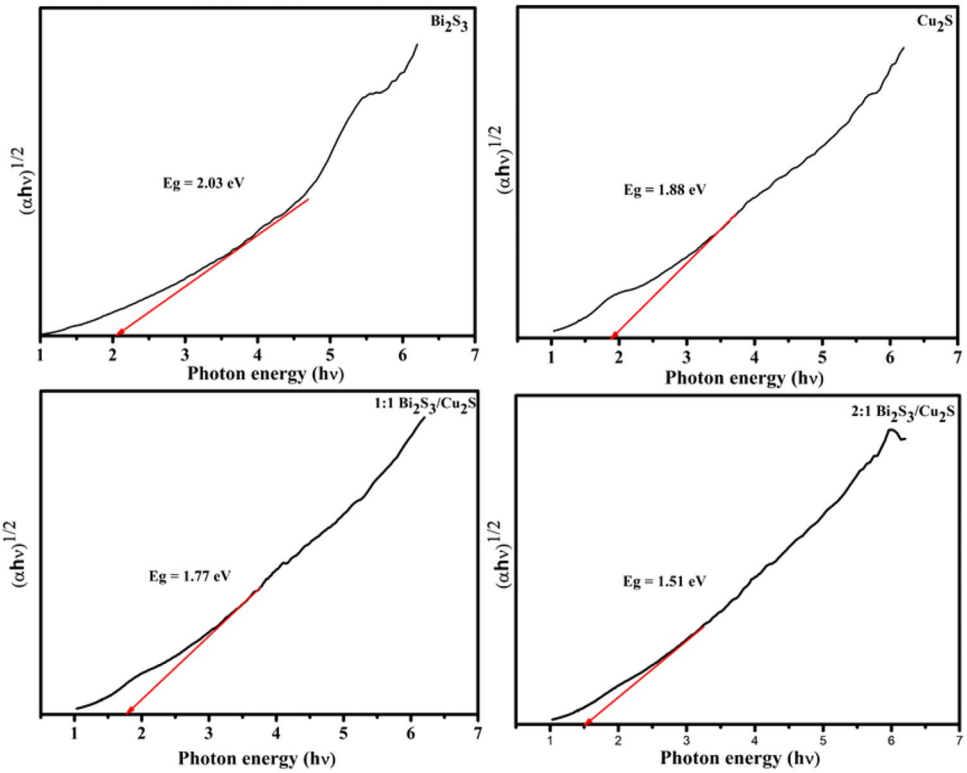

Fig. 4 Band gap energy (Tauc plot) of as-prepared nanocomposites

eV and 164.8 eV, which can be attributed to Bi^{3+} (Geng et al. 2017), in addition the peaks observed at 445.2 eV and 465 eV correspond to Bi4d3/2 and Bi4d5/2, respectively (Geng et al. 2021). The observed carbon peak at 285.1 eV for binding energy is ascribed to carbon present in grid used for XPS analysis. The S 2p region is defined by two asymmetric peaks, S $2p^{3/2}$ is responsible for the highest intensity peak approximately at 165 eV and the spin state of S $2p^{1/2}$

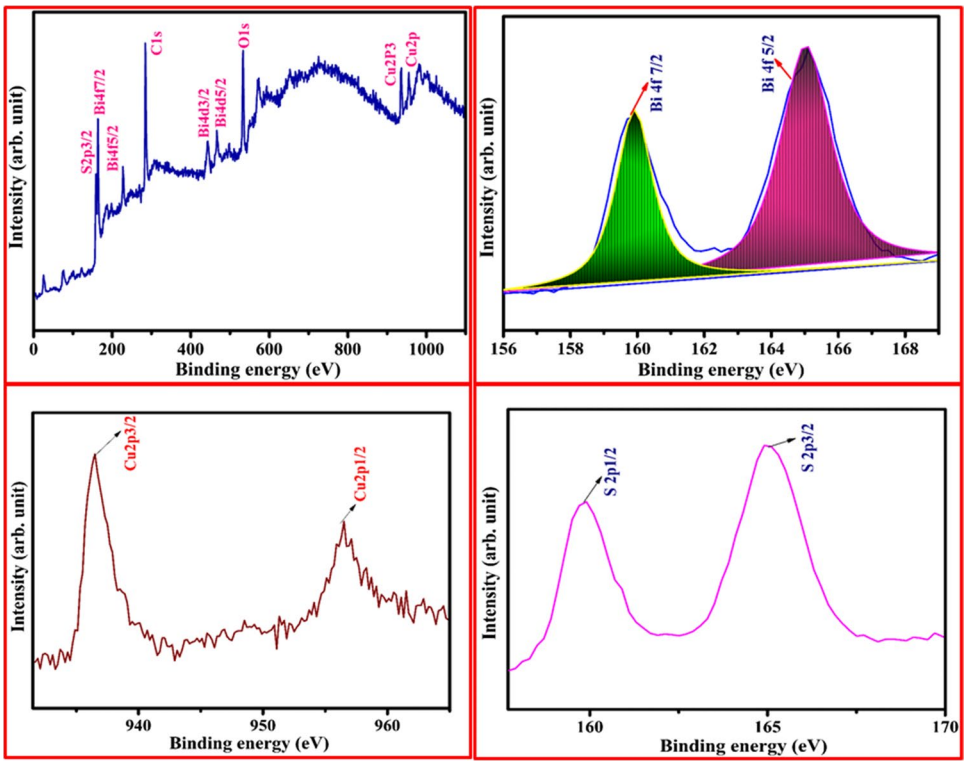

Fig. 5 XPS spectra of (2:1) Bi_2S_3/Cu_2S nanocomposites. **a** Survey spectra, **b** Bi 4f, **c** Cu 2p, and **d** S 2p

is responsible for the small peak at 159.8 eV (Grigas et al. 2008). Cu 2p1/2 and 2p3/2 binding energies were evaluated to be 956.53 and 936.46 eV, respectively (Hassanien et al. 2016), representing the presence of copper in the active catalysts. It can be conclude that the Bi_2S_3/Cu_2S heterojunction formation has been successfully synthesized on the basis of above the analysis results of PXRD, HRTEM, and XPS.

Photocatalytic application

The photocatalytic degradation activities for MB dye and TC drug over the composite samples with different Bi_2S_3 contents were carried out under visible light irradiation. Figure 6a clearly shows that the maximal absorption peak of MB dye was noticed at 664 nm, and Fig. 6b shows the maximal absorption peak of the TC drug at 360 nm, which is similar to the previous research articles. Compared to other samples, the (2:1) $Bi2S_3/Cu_2S$ nanocomposites showed superior UV-visible degradation efficiency in 60 min for both the MB dye and the TC drug. The ability for photocatalytic degradation of (2:1) Bi_2S_3/Cu_2S nanocomposites was significantly higher; this would be explained by improved visible light absorption and the synergistic effect of as-prepared nanocomposites.

The kinetics of MB dye degradation were investigated by fitting a pseudo-first-order kinetics equation to all samples that followed the equation (Park 2010).

$$\ln = \left(C/C_0\right) = Kt \tag{3}$$

Figure 7a shows the absorbance peak intensity with increasing irradiation time. It was shown that the absorbance of dye was gradually degrading under visible light irradiation in presence of the as-prepared samples. The experiments conducted in the absence of photocatalytst and under dark conditions from −30 to 0 min indicate that the elimination of MB dye is less than 10%. As a result, the impact of light and absorption/desorption alone on the MB dye can be considered negligible. The MB dye kinetics was adapted to a pseudo-first-order kinetic model, and the photocatalytic performance of the MB dye decomposition reaction using various photocatalysts shows a linear relationship between time and $\ln(C/C_0)$ depicted in Fig. 7b. From Fig. 7c, it shows that the photocatalytic degradation efficiencies of MB dye over Bi_2S_3, CuS_2, (1:1) Bi_2S_3/Cu_2S, and (2:1) Bi_2S_3/Cu_2S nanocomposites are 88.3, 54.4, 78, and 90.2%, respectively. Table 1 shows the detailed information about comparison with other photocatalysts for the MB dye TC drug degradation under various reaction time and various catalysts.

In Fig. 7d, it is confirmed that reactive species such as electrons play a minor role in MB dye degradation; these findings show that hydroxyl radicals and superoxide radicals, rather than electrons, are the major reactive oxygen species during the photodegradation of MB dye under visible light illumination. The degradation of tetracycline drugs in the presence of as-prepared photocatalysts under UV-visible light irradiation was studied using a similar MB dye degradation process, as shown in Fig. 8a. In Fig. 8b, the pseudo-first-order kinetic model was used to prove the mathematical confirmation of tetracycline degradation; the as-prepared photocatalysts showed better linear performance and are properly fitted into the pseudo-first-order kinetic reaction model. In Fig. 8c, the photodegradation efficiencies of tetracycline drug over Bi_2S_3, Cu_2S, Bi_2S_3/Cu_2S (1:1), and Bi_2S_3/Cu_2S (2:1) nanocomposites are 56, 73, 56, and 87.5%, respectively. Based on the results, it is clear that Bi_2S_3/Cu_2S (2:1) photocatalysts exhibit enhanced photocatalytic performance on tetracycline drug degradation due to the interfacial between Bi_2S_3 and Cu_2S nanoparticles.

Possible mechanism of photocatalytic degradation

The proposed photocatalytic mechanism of the as-prepared photocatalysts in the photocatalytic experimental process depicts in Fig. 9. When the light was exposed to UV-light irradiation with photocatalysts, the electrons

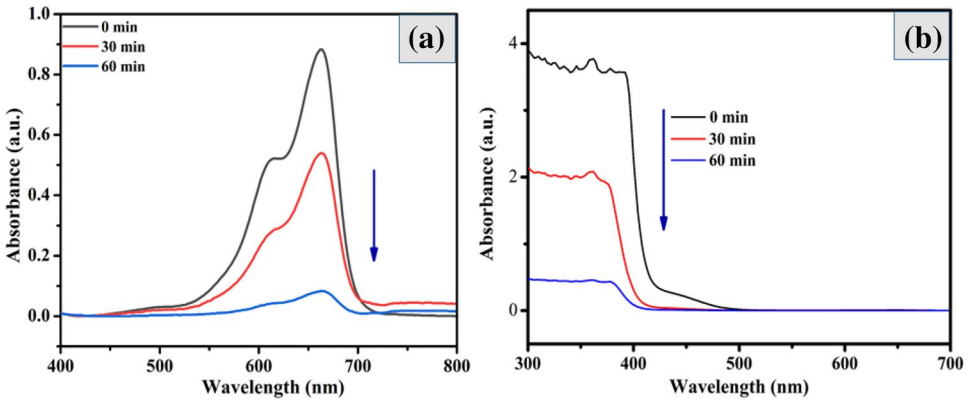

Fig. 6 Photocatalytic performance of (2:1) Bi_2S_3/Cu_2S nanocomposites evaluated against **a** MB dye and **b** TC drug

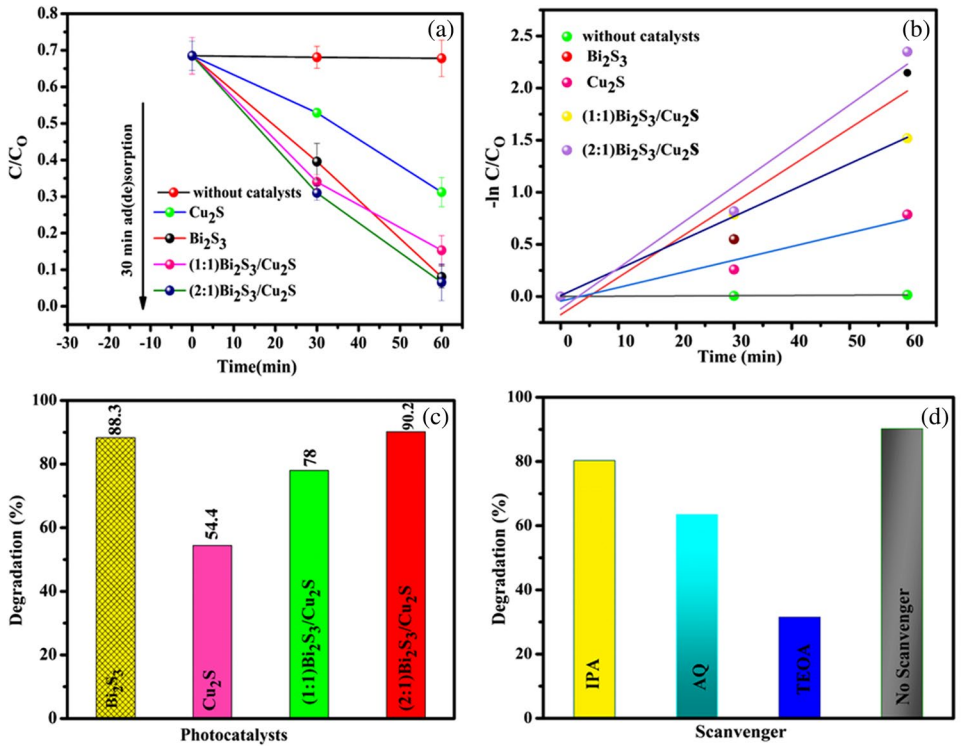

Fig. 7 **a** Photocatalytic performance, **b** pseudo first order kinetic model, **c** degradation efficiency of as-prepared nanocomposites, and **d** scavenger test of as-prepared Bi_2S_3/Cu_2S nanocomposites against MB dye

Table 1 Comparison with other photocatalysts for the MB dye and TC drug degradation

S.no	Sample	Dye and drug	Degradation efficiency	Reaction time (min)	References
1	$Cu_2O/BiVO_4$	MB	72.19	160	(Min et al. 2014)
2	CeO_2/V_2O_5	MB	76.9	300	(Song et al. 2012)
3	CeO_2/CuO	MB	85.7	300	(Saravanan et al. 2013)
4	Bi_2S_3/Cu_2S	MB	90.2	60	Present work
5	$ZnO/BiVO_4$	TC	60	60	(Li et al. 2021)
6	$AgCl/BiVO_4$	TC	77	120	(Ma et al. 2021)
7	$g\text{-}C_3N_4/BiVO_4$	TC	60	60	(Kang et al. 2021)
8	$g\text{-}C_3N_4/BiVO_4$ + Pms	TC	60	60	(Kang et al. 2021)
9	Bi_2S_3/Cu_2S	TC	87.5	60	Present work

were photoexcited from the valence band to the conduction band. In general, three steps are involved in photocatalytic mechanisms: in the first step, dye molecules can move from the aqueous to the outer surface of the catalysts. In the second step, dye molecules are adsorbed from the outer layer to the interior pores of the catalysts, a process known as intra-particle diffusion. Finally, dye molecules interact with the internal pores active sites of the catalyst in the third step. The photogenerated electrons and holes interacted with water molecules and produce the superoxide radical ($*O_2^{\cdot}$) and hydroxyl radical ($*OH^-$), respectively. Meanwhile, the holes formed in the VB of Bi_2S_3 can be selectively oxidized by the surface $*OH^-$ anions H_2O molecule to form hydroxyl radicals $*OH^-$. On the other side, Cu_2S plays a minor role, in which electrons are considered a difficult way to excite from VB to CB. The produced active O_2 and $*OH^-$ species could then degrade the MB into small harmless products such as CO_2, H_2O, and so on.

Stability test

One of the most important aspects of the practical use of as-prepared photocatalysts is their stability and reuse performance; hence, the recycling performance of Bi_2S_3/Cu_2S (2:1) nanocomposites is carried up to five consecutive cycles and the results are shown in Fig. 10a and b. Each cycle was run for 60 min, subsequently, during each run, the reaction photocatalyst was collected and washed with several time ethanol and DDW. Eventually,

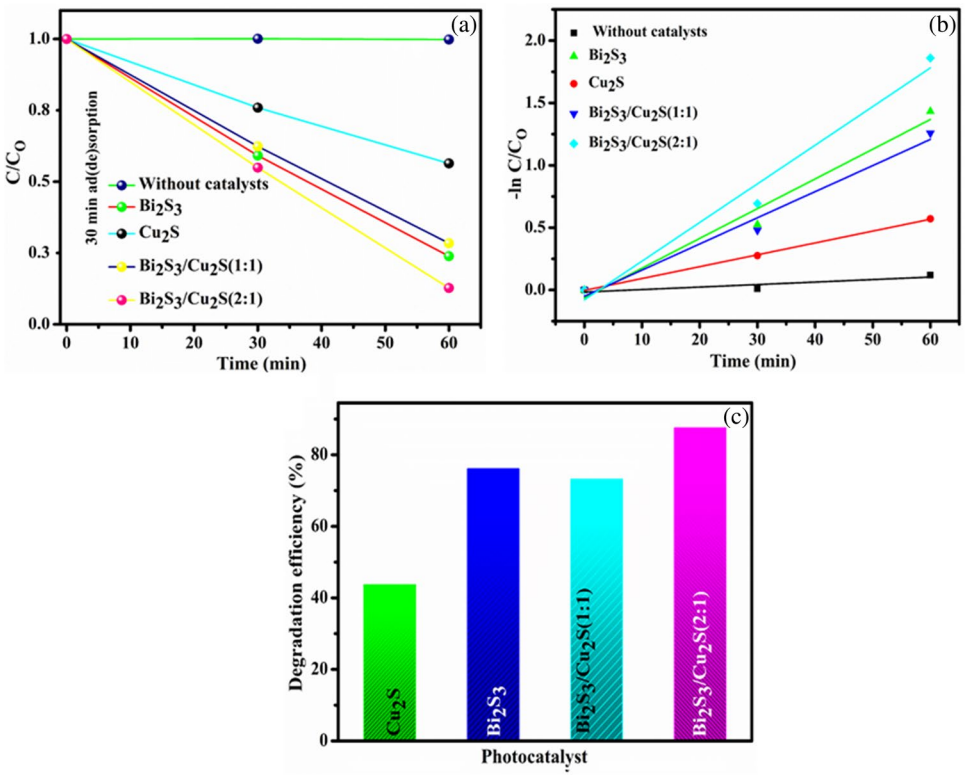

Fig. 8 **a** Photocatalytic performance, **b** pseudo-first-order kinetic model, and **c** degradation efficiency of as-prepared nanocomposites against TC dye

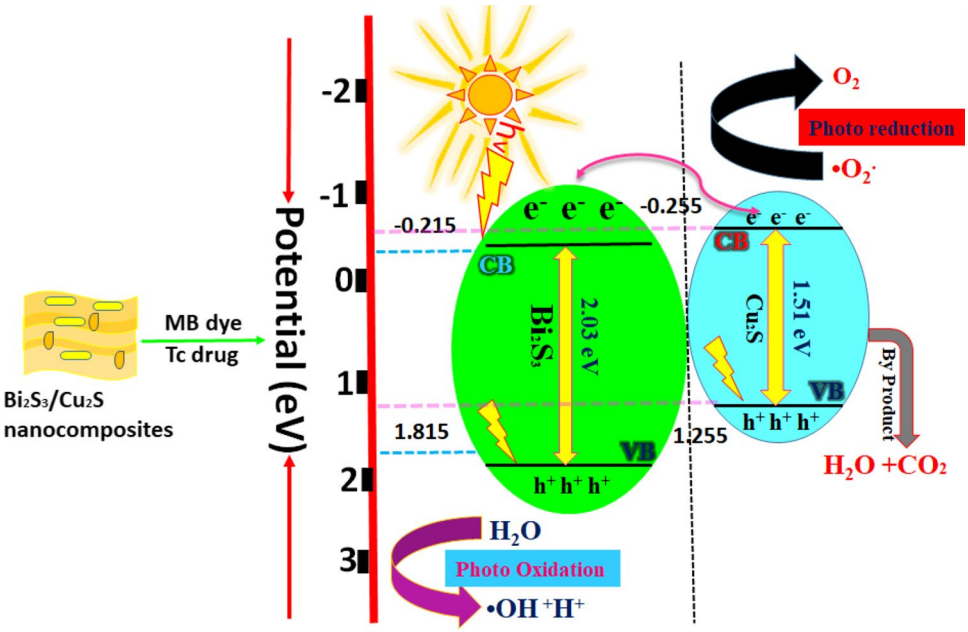

Fig. 9 A possible photocatalytic degradation mechanism of Bi_2S_3/Cu_2S nanocomposites against MB dye and TC drug degradation

the collected photocatalysts were dried at 80 °C overnight. The photodegradation efficiency of MB dye was decreased from 90.5 to 87.64% while tetracycline drugs reduced efficacy from 87.5 to 84.87%, respectively. This decrease in efficiency could be due to catalyst losses during the recovery process.

Figure 11a and b depict the XRD and FTIR spectra before and after the photocatalytic experiment. The observed results show similar characteristics peaks as fresh samples and no other substance or functional groups were observed in the results. The above findings' results show that (2:1) Bi_2S_3/Cu_2S nanocomposites have excellent stability.

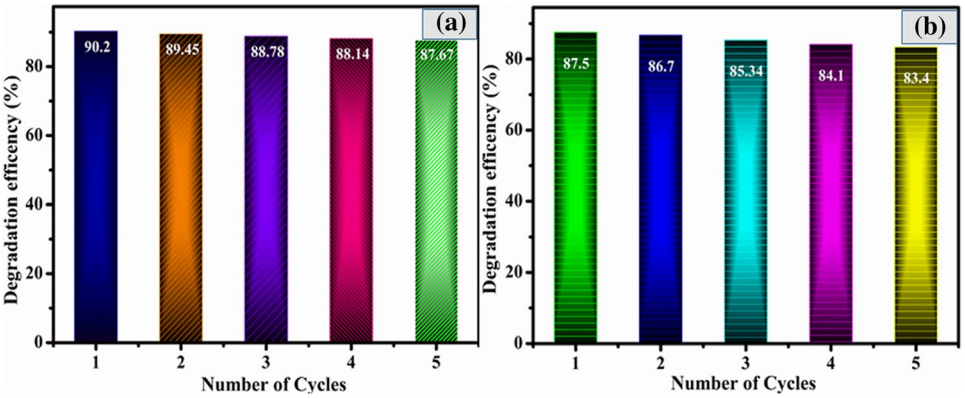

Fig. 10 Recycle run for the photocatalytic degradation of **a** MB dye and **b** TC drug over as-prepared (2:1) Bi_2S_3/Cu_2S nanocomposites

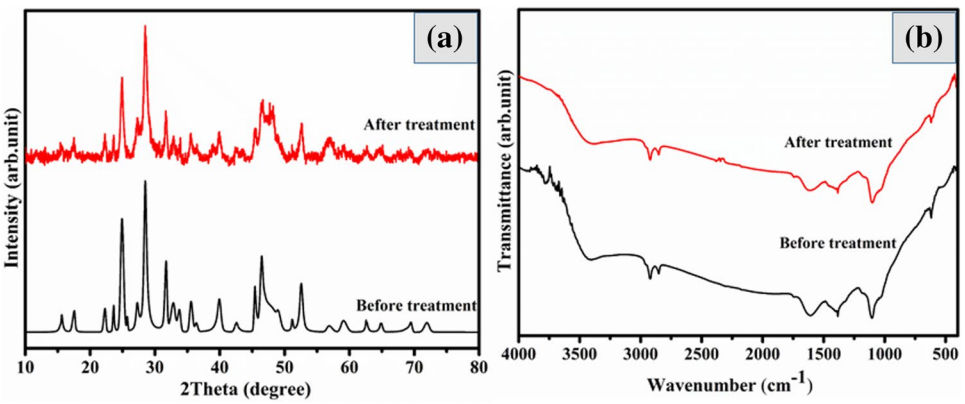

Fig. 11 **a** XRD pattern and **b** FTIR spectra for as-prepared (2:1) Bi_2S_3/Cu_2S nanocomposites before and after 5 cyclic runs

Conclusion

In summary, Bi_2S_3/Cu_2S nanocomposites have been successfully prepared via a hydrothermal method and characterized using various instrumental techniques, such as XRD, FTIR, UV DRS, SEM, EDS mapping, HRTEM, and XPS analysis. The maximum MB dye and TC drug degradation efficiency of 90.2% and 87.5% was achieved within 60 min of UV-visible light irradiation over (2:1) Bi_2S_3/Cu_2S nanocomposites. As consistent with the experimental degradation result, the (2:1) Bi_2S_3/Cu_2S nanocomposites system follows pseudo first order kinetic and these binary composites exhibit significantly improved rate constant, as compared to other samples. The trapping experiment confirmed that OH* radicals were the major species for the degradation of MB and TC in the photocatalytic process. The possible photocatalytic reaction mechanism was discussed based on the trapping results, with the observation that the formation of a Bi_2S_3/Cu_2S heterojunction increased the generation of free electrons, thereby allowing for greater participation of holes in the formation of OH* radicals. Also, it was noticeable that the Bi_2S_3/Cu_2S photocatalysts could be reused for five consecutive runs without any significant decrease in their photocatalytic activity. All the experiments have shown that hybrid photocatalysts based on Bi_2S_3 and Cu_2S are suitable for the removal of various organic pollutants, resulting in an optimized proposal. The photocatalytic degradation activity of Bi_2S_3/Cu_2S nanoparticles can be enhanced by decreasing their size, which will increase their surface area and increase their photoactive surfaces.

Supplementary Information The online version contains supplementary material available at https://doi.org/10.1007/s11356-023-26627-9.

Author contribution Balaji Parasuraman: conceptualization, investigation, writing — original draft, and visualization. Vasanthakumar Vasudevan: data curation, validation, investigation, and formal analysis. Bhuvaneswari Kandasamy: visualization, investigation, and formal analysis. Hariprasath Rangaraju: methodology, data curation, validation, and formal analysis. Pazhanivel Thangavelu: conceptualization, supervision, visualization, project administration, and formal analysis.

Data availability The datasets used and analyzed during the current study are available from the corresponding author on reasonable request.

Declarations

Ethics approval and consent to participate Not applicable.

Consent for publication Not applicable.

Competing interests The authors declare no competing interests.

References

Ajiboye TO, Onwudiwe DC (2021) Bismuth sulfide based compounds: Properties, synthesis and applications. Results Chem 3. https://doi.org/10.1016/j.rechem.2021.100151

Akhavan O, Abdolahad M, Esfandiar A, Mohatashamifar M (2010) Photodegradation of graphene oxide sheets by TiO2 nanoparticles after a photocatalytic reduction. J Phys Chem C 114:12955–12959. https://doi.org/10.1021/jp103472c

Ali AA, Nazeer AA, Madkour M et al (2018) Novel supercapacitor electrodes based semiconductor nanoheterostructure of CdS/rGO/CeO2 as efficient candidates. Arab J Chem 11:692–699. https://doi.org/10.1016/j.arabjc.2018.03.010

Arumugam J, Dhayal Raj A, Albert Irudayaraj A (2017) Solvent effects on the properties of Bi2S3 nanoparticles: photocatalytic application. J Mater Sci Mater Electron 28:3487–3494. https://doi.org/10.1007/s10854-016-5947-6

Bharathi P, Harish S, Archana J et al (2019) Enhanced charge transfer and separation of hierarchical CuO/ZnO composites: the synergistic effect of photocatalysis for the mineralization of organic pollutant in water. Appl Surf Sci 484:884–891. https://doi.org/10.1016/j.apsusc.2019.03.131

Bhuvaneswari K, Palanisamy G, Pazhanivel T, et al (2021a) In-situ development of metal organic frameworks assisted ZnMgAl layered triple hydroxide 2D/2D hybrid as an efficient photocatalyst for organic dye degradation. Chemosphere 270. https://doi.org/10.1016/j.chemosphere.2020.128616

Bhuvaneswari K, Palanisamy G, Sivashanmugan K, et al (2021b) ZnO nanoparticles decorated multiwall carbon nanotube assisted ZnMgAl layered triple hydroxide hybrid photocatalyst for visible light-driven organic pollutants removal. J Environ Chem Eng 9. https://doi.org/10.1016/j.jece.2020.104909

Chaniotakis N, Sofikiti N (2008) Novel semiconductor materials for the development of chemical sensors and biosensors: a review. Anal Chim Acta 615:1–9

Chong MN, Jin B, Chow CWK, Saint C (2010) Recent developments in photocatalytic water treatment technology: a review. Water Res 44:2997–3027

Cui L, Ding X, Wang Y et al (2017) Facile preparation of Z-scheme WO_3/g-C_3N_4 composite photocatalyst with enhanced photocatalytic performance under visible light. Appl Surf Sci 391:202–210. https://doi.org/10.1016/j.apsusc.2016.07.055

Dadigala R, Bandi R, Gangapuram BR, Guttena V (2019) Construction of in situ self-assembled $FeWO_4$/g-C_3N_4 nanosheet heterostructured Z-scheme photocatalysts for enhanced photocatalytic degradation of rhodamine B and tetracycline. Nanoscale Adv 1:322–333. https://doi.org/10.1039/c8na00041g

Danish M, Tayyab M, Akhtar A, et al (2020) Effect of soft template variation on the synthesis, physical, and electrochemical properties of Mn3O4 nanomaterial. Inorg Nano-Metal Chem 1–7. https://doi.org/10.1080/24701556.2020.1790000

Das S, Ahn YH (2022) Synthesis and application of CdS nanorods for LED-based photocatalytic degradation of tetracycline antibiotic. Chemosphere 291. https://doi.org/10.1016/j.chemosphere.2021.132870

Ebrahimi M, Akhavan O (2022) Nanomaterials for photocatalytic degradations of analgesic, mucolytic and anti-biotic/viral/inflammatory drugs widely used in controlling SARS-CoV-2. Catalysts 12. https://doi.org/10.3390/catal12060667

Elango G, Roopan SM (2016) Efficacy of SnO_2 nanoparticles toward photocatalytic degradation of methylene blue dye. J Photochem Photobiol B Biol 155:34–38. https://doi.org/10.1016/j.jphotobiol.2015.12.010

Elmetwally AE, Goodarzi F, Meier KK et al (2021) Cu_2S@Bi_2S_3 double-shelled hollow cages as a nanocatalyst with substantial activity in peroxymonosulfate activation for atrazine degradation. ACS Appl Nano Mater 4:12222–12234. https://doi.org/10.1021/acsanm.1c02741

Geng X, Zhang D, Zheng Z, et al (2021) Integrated multifunctional device based on Bi2S3/Pd: localized heat channeling for efficient photothermic vaporization and real-time health monitoring. Nano Energy 82. https://doi.org/10.1016/j.nanoen.2020.105700

Geng Z, Li K, Li X, Shi D (2017) Fabrication and photoluminescence of Eu-doped KNN-based transparent ceramics. J Mater Sci 52:2285–2295. https://doi.org/10.1007/s10853-016-0521-4

Grigas J, Talik E, Lazauskas V et al (2008) XPS and electronic structure of ferroelectric sn2p 2s6 crystals. Lith J Phys 48:145–154. https://doi.org/10.3952/lithjphys.48205

Hariharan C (2006) Photocatalytic degradation of organic contaminants in water by ZnO nanoparticles: revisited. Appl Catal A Gen 304:55–61. https://doi.org/10.1016/j.apcata.2006.02.020

Hassanien R, Almaky MM, Houlton A, Horrocks BR (2016) Preparation and electrical properties of a copper-conductive polymer hybrid nanostructure. RSC Adv 6:99422–99432. https://doi.org/10.1039/c6ra20325f

He X, Wu P, Wang S, Wang A, Wang C, Ding P (2021) Inactivation of harmful algae using photocatalysts: Mechanisms and performance. J Clean Prod 289. https://doi.org/10.1016/j.jclepro.2020.125755

Jada N, Sankaran KJ, Sakthivel R, et al (2021) Synergistic effect of MoO_3/TiO_2 towards discrete and simultaneous photocatalytic degradation of E. coli and methylene blue in water. Bull Mater Sci 44. https://doi.org/10.1007/s12034-021-02436-z

Jia J, Jiang C, Zhang X, et al (2019) Urea-modified carbon quantum dots as electron mediator decorated g-C_3N_4/WO_3 with enhanced visible-light photocatalytic activity and mechanism insight. Appl Surf Sci 495. https://doi.org/10.1016/j.apsusc.2019.07.266

Kang J, Tang Y, Wang M, et al (2021) The enhanced peroxymonosulfate-assisted photocatalytic degradation of tetracycline under visible light by g-C_3N_4/Na-$BiVO_4$heterojunction catalyst and its mechanism. J Environ Chem Eng 9:. https://doi.org/10.1016/j.jece.2021.105524

Kumar V, Chauhan V, Ram J, et al (2020) Study of humidity sensing properties and ion beam induced modifications in SnO_2-TiO_2 nanocomposite thin films. Surf Coatings Technol 392. https://doi.org/10.1016/j.surfcoat.2020.125768

Kuo TR, Liao HJ, Chen YT et al (2018) Extended visible to near-infrared harvesting of earth-abundant FeS_2-TiO_2 heterostructures for highly active photocatalytic hydrogen evolution. Green Chem 20:1640–1647. https://doi.org/10.1039/c7gc03173d

Li R, Jia Y, Bu N et al (2015) Photocatalytic degradation of methyl blue using Fe2O3/TiO2 composite ceramics. J Alloys Compd 643:88–93. https://doi.org/10.1016/j.jallcom.2015.03.266

Li Y, Sun X, Tang Y, et al (2021) Understanding photoelectrocatalytic degradation of tetracycline over three-dimensional coral-like ZnO/$BiVO_4$ nanocomposite. Mater Chem Phys 271. https://doi.org/10.1016/j.matchemphys.2021.124871

Liu G, Feng M, Tayyab M, et al (2021a) Direct and efficient reduction of perfluorooctanoic acid using bimetallic catalyst supported on carbon. J Hazard Mater 412. https://doi.org/10.1016/j.jhazmat.2021.125224

Liu W, Wang M, Xu C et al (2013) Ag_3PO_4/ZnO: an efficient visible-light-sensitized composite with its application in photocatalytic degradation of rhodamine B. Mater Res Bull 48:106–113. https://doi.org/10.1016/j.materresbull.2012.10.015

Liu Y, Zhu Q, Tayyab M, et al (2021b) Single-atom Pt loaded zinc vacancies ZnO–ZnS induced type-V electron transport for efficiency photocatalytic H2 evolution. Sol RRL 5. https://doi.org/10.1002/solr.202100536

Ma C, Din STU, Seo WC, et al (2021) $BiVO_4$ ternary photocatalyst co-modified with N-doped graphene nanodots and Ag nanoparticles for improved photocatalytic oxidation: a significant enhancement in photoinduced carrier separation and broad-spectrum light

absorption. Sep Purif Technol 264. https://doi.org/10.1016/j.seppur.2021.118423
Ma L, Zhao Q, Zhang Q et al (2014) Controlled assembly of Bi_2S_3 architectures as Schottky diode, supercapacitor electrodes and highly efficient photocatalysts. RSC Adv 40:41636–41641. https://doi.org/10.1039/c4ra07169g
Mahmoodi NM, Arami M, Limaee NY, Tabrizi NS (2006) Kinetics of heterogeneous photocatalytic degradation of reactive dyes in an immobilized TiO_2 photocatalytic reactor. J Colloid Interface Sci 295:159–164. https://doi.org/10.1016/j.jcis.2005.08.007
Majumder S, Chatterjee S, Basnet P, Mukherjee J (2020) ZnO based nanomaterials for photocatalytic degradation of aqueous pharmaceutical waste solutions – A contemporary review. Environ. Nanotechnol Monit Manag 14. https://doi.org/10.1016/j.enmm.2020.100386
Marimuthu G, Nguyen BS, Pham VT, et al (2021) Novel $NiCo_2O_4$/MWCNTs nanocomposite with flake-like architecture as room temperature capacitive-type NH3 gas sensor. Mater Lett 283. https://doi.org/10.1016/j.matlet.2020.128814
Min S, Wang F, Jin Z, Xu J (2014) Cu2O nanoparticles decorated $BiVO_4$ as an effective visible-light-driven p-n heterojunction photocatalyst for methylene blue degradation. Superlattices Microstruct 74:294–307. https://doi.org/10.1016/j.spmi.2014.07.003
Mondal G, Jana S, Santra A et al (2015) Single-source mediated facile electrosynthesis of p-Cu2S thin films on TCO (SnO_2:F) with enhanced photocatalytic activities. RSC Adv 5:52235–52242. https://doi.org/10.1039/c5ra06102d
Moradeeya PG, Sharma A, Kumar MA, Basha S (2022) Titanium dioxide based nanocomposites – current trends and emerging strategies for the photocatalytic degradation of ruinous environmental pollutants. Environ Res 204. https://doi.org/10.1016/j.envres.2021.112384
Mrunal VK, Vishnu AK, Momin N, Manjanna J (2019) Cu_2O nanoparticles for adsorption and photocatalytic degradation of methylene blue dye from aqueous medium. Environ Nanotechnology, Monit Manag 12. https://doi.org/10.1016/j.enmm.2019.100265
Nourmohammadi A, Rahighi R, Akhavan O, Moshfegh A (2014) Graphene oxide sheets involved in vertically aligned zinc oxide nanowires for visible light photoinactivation of bacteria. J Alloys Compd 612:380–385. https://doi.org/10.1016/j.jallcom.2014.05.195
Oluwole AO, Omotola EO, Olatunji OS (2020) Pharmaceuticals and personal care products in water and wastewater: a review of treatment processes and use of photocatalyst immobilized on functionalized carbon in AOP degradation. BMC Chem 14. https://doi.org/10.1186/s13065-020-00714-1
Palanisamy G, Bhuvaneswari K, Pazhanivel T, Bharathi G (2020) Enriched photocatalytic activity of rhodamine B dye from aqueous solution using hollow sphere tungsten trioxide nanoparticles. Optik (Stuttg) 204. https://doi.org/10.1016/j.ijleo.2020.164171
Park J (2010) Photocatalytic activity of hydroxyapatite-precipitated potassium titanate whiskers. J Alloys Compd 492. https://doi.org/10.1016/j.jallcom.2009.11.172
Rajendran R, Varadharajan K, Jayaraman V et al (2018) Photocatalytic degradation of metronidazole and methylene blue by PVA-assisted Bi_2WO_6-CdS nanocomposite film under visible light irradiation. Appl Nanosci 8:61–78. https://doi.org/10.1007/s13204-018-0652-9
Ravikumar S, Mani D, Rizwan Khan M, et al (2022) Effect of silver incorporation on the photocatalytic degradation of Reactive Red 120 using ZnS nanoparticles under UV and solar light irradiation. Environ Res 209. https://doi.org/10.1016/j.envres.2022.112819
Saadati M, Akhavan O, Fazli H (2021) Single-layer MoS2-MoO3-x heterojunction nanosheets with simultaneous photoluminescence and co-photocatalytic features. Catalysts 11. https://doi.org/10.3390/catal11121445
Saravanan R, Joicy S, Gupta VK et al (2013) Visible light induced degradation of methylene blue using CeO_2/V_2O_5 and CeO_2/CuO catalysts. Mater Sci Eng C 33:4725–4731. https://doi.org/10.1016/j.msec.2013.07.034
Shchukin D, Poznyak S, Kulak A, Pichat P (2004) TiO_2-In_2O_3 photocatalysts: preparation, characterisations and activity for 2-chlorophenol degradation in water. J Photochem Photobiol A Chem 162:423–430. https://doi.org/10.1016/S1010-6030(03)00386-1
Song L, Zhang S, Wu X, Wei Q (2012) A metal-free and graphitic carbon nitride sonocatalyst with high sonocatalytic activity for degradation methylene blue. Chem Eng J 184:256–260. https://doi.org/10.1016/j.cej.2012.01.053
Sonkusare VN, Chaudhary RG, Bhusari GS et al (2018) Microwave-mediated synthesis, photocatalytic degradation and antibacterial activity of α-Bi_2O_3 microflowers/novel γ-Bi2O3 microspindles. Nano-Structures and Nano-Objects 13:121–131. https://doi.org/10.1016/j.nanoso.2018.01.002
Tayyab M, Liu Y, Liu Z et al (2022a) One-pot in-situ hydrothermal synthesis of ternary In2S3/Nb2O5/Nb2C Schottky/S-scheme integrated heterojunction for efficient photocatalytic hydrogen production. J Colloid Interface Sci 628:500–512. https://doi.org/10.1016/j.jcis.2022.08.071
Tayyab M, Liu Y, Liu Z et al (2022b) A new breakthrough in photocatalytic hydrogen evolution by amorphous and chalcogenide enriched cocatalysts. Chem Eng J. https://doi.org/10.1016/j.cej.2022.140601
Tayyab M, Liu Y, Min S et al (2022c) Simultaneous hydrogen production with the selective oxidation of benzyl alcohol to benzaldehyde by a noble-metal-free photocatalyst VC/CdS nanowires. Chinese J Catal 43:1165–1175. https://doi.org/10.1016/S1872-2067(21)63997-9
Wei L, Yu C, Zhang Q et al (2018) TiO2-based heterojunction photocatalysts for photocatalytic reduction of CO_2 into solar fuels. J Mater Chem A 6:22411–22436
Xu W, Zhu S, Liang Y, et al (2015) Nanoporous CuS with excellent photocatalytic property. Sci Rep 5. https://doi.org/10.1038/srep18125
Ye Z, Yue W, Tayyab M et al (2022) Simple one-pot, high-yield synthesis of 2D graphitic carbon nitride nanosheets for photocatalytic hydrogen production. Dalt Trans 51:18542–18548. https://doi.org/10.1039/d2dt03272d
Yu J, Yu C, Yu H (2022) Preface to special issue for the 3rd Chinese Symposium on Photocatalytic Materials (CSPM3). Chinese J Catal 43:177
Zhao D, Wang W, Zong W, et al (2017) Synthesis of Bi_2S_3 /BiVO heterojunction with a one-step hydrothermal method based on pH control and the evaluation of visible-light photocatalytic performance. Materials (Basel) 10. https://doi.org/10.3390/ma10080891
Zhou J, Tian G, Chen Y, et al (2014) Growth rate controlled synthesis of hierarchical Bi2S 3/In2S3 core/shell microspheres with enhanced photocatalytic activity. Sci Rep 4. https://doi.org/10.1038/srep04027
Zhu J, Zhou M, Xu J, Liao X (2001) Preparation of CdS and ZnS nanoparticles using microwave irradiation. Mater Lett 47:25–29. https://doi.org/10.1016/S0167-577X(00)00206-8